RSC Advances

ROYAL SOCIETY OF CHEMISTRY

www.rsc.org/advances

Electrospun Carbon Nitride Supported On Poly(vinyl) Alcohol As An Electrocatalyst For Oxygen Reduction Reaction

Amandeep Jindal[a], Suddhasatwa Basu[a]* and Aby C.P[b]

[a] Department of Chemical Engineering, Indian Institute of Technology Delhi, New Delhi 110016, India

[b] Bio-Nano Electronics Research Centre, Toyo University, Kawagoe, Saitama, 350 - 8585, Japan

*Corresponding author: tel +91 11 26591021; fax +91 11 26581120 email: sbasu@chemical.iitd.ac.in

Abstract

Electrochemical oxygen reduction reaction (ORR) via nonprecious catalysts has the potential for significant cost reduction in fuel cells. Dense, multi-layered poly(vinyl) alcohol (PVA) nanofibers dispersed with catalytically active carbon nitride (CN_x) nanoparticles were synthesized using electrospinning process. Size, morphology, elemental composition, bond structure of the CN_x/PVA nanofibers were analysed using TEM, SEM, FTIR, XPS and Raman spectroscopic studies. Significant improvement in the electrocatalytic activity of CN_x nanoparticles dispersed in the nanofibers as compared to its native form was observed towards ORR by voltammetry coupled with FTIR studies. Onset potential and peak current density observed for CN_x/PVA nanofibers using cyclic voltammetry was comparable to conventional Pt/C (40:60 % by weight) catalyst. ORR mechanism was further analysed using RRDE and *in-situ* FTIR with linear sweep voltammetry studies. RRDE analysis confirmed that ORR takes place primarily via 4-electron pathway. The catalytic activity of CN_x/PVA nanofibers for ORR was stable over 5000 repetitions of voltammetric studies coupled with FTIR.

Keywords: Carbon nitride, nanofiber, oxygen reduction reaction, electrospinning

1. Introduction

In recent years, the research interest in fuel cells has been increased as it is a promising energy device not only due to its wide range of applications but also due to its numerous advantages over conventional energy devices[1]. Oxygen reduction reaction (ORR), being the slowest reaction, is the heart of studies for the development of cathode catalysts as it

dominates the overall performance of the proton exchnge membrane fuel cell. Till date, catalysts that have been proved to be the best for ORR contain platinum. However, certain factors such as CO poisoning, Pt scarcity and above all, high cost are a big obstacles in the commercialisation of fuel cells[2–4]. Hence, recent focus of research is shifted to non-platinum catalyst materials[5–8]. In nitrogen rich carbon atoms, ORR occurs via more efficient one step 4-electron pathway in acid medium[4,9–11]. High electron affinity of adjoining nitrogen atom induces positive charge density on carbon atoms. It improves the adsorption of oxygen on carbon atoms and thus weakens the inherent oxygen bonding facilitating 4-electron transfer in ORR[12].

Carbon nitride (CN_x) as a nitrogen rich carbon material is highly stable, oxidation resistant and it can be used as an economically viable catalyst for ORR, but requires further improvement[4,9-13]. Agglomeration and low surface area limit its catalytic application[14]. In order to enhance its activity, CN_x nanoparticles are uniformly dispersed and embedded in polyvinyl alcohol (PVA) nanofibers using electrospinning technique[15–17]. There are different techniques to prepare CN_x nanofibers and nanotubes using various methods such as template methods[18–21] and direct pyrolysis of the precursors ferrocene/melamine mixtures[16]. Template method has the drawback of making continuous nanofibers[22]. Pyrolysis involves difficulty in the preparation of CN_x structure in the nanofiber matrix[16]. It is evident from recent research studies that electrospinning has unique advantages over nanofibres formed by other methods[22–27]. In electrospinning, nanofibers are prepared from a polymer solution, e.g., PVA and the electrostatic field stretches the polymer solution into fibers as the solvent is evaporated. PVA is chemically and thermally stable, non-toxic and hydrophilic in nature. Its flexibility and toughness characteristics augment physical properties of the nanofibers[28].

Nanofibers composed of CN_x nanoparticles have been synthesized using electrospinning technique and tested for ORR. PVA is chosen as the supporting polymer because of its elastic property and conducive to electrospinning as mentioned above. Physical characterizations are carried out for both CN_x nanoparticles and nanofibers to understand morphology, elemental analysis and bond structure. The catalytic activity of CN_x nanofibers over native CN_x nanoparticles are observed using voltammetry and compared with the catalytic activity of conventional Pt/C (40:60 % by weight) catalyst. ORR mechanism is analysed using RRDE and in-situ FTIR studies combined with voltammetry.

2. Experimental

2.1. Materials

Ethylene diamine (Merck) and carbon tetrachloride (Merck) were used as precursors for the preparation of carbon nitride. Ethanol (Merck) was used to wash the carbon nitride nanoparticles formed. Poly(vinyl) alcohol (Molecular weight: 85,000 to 1,24,000, Sigma Aldrich) was used as the supporting polymer to enable electrospinning of carbon nitride. Deionized water (18.2 MΩ cm) was used as solvent for electrospinning. Two-propanol (Merck) was used to disperse carbon nitride nanoparticles and Pt/C (Alfa Aesar) to make catalyst ink. Nafion® dispersion (DE-521, DuPont, USA) was used as a binder. Commercial platinum/carbon (Pt/C) (Pt loading: 40 wt. %, Pt on carbon black) was purchased from Alfa Aesar.

2.2. Preparation of CN_x nanoparticles

Carbon nitride was prepared from the chemical precursors ethylene diamine (EDA) and carbon tetrachloride (CCl_4) using the method proposed by Qiu et al.[29, 30]. At first 110 mL of EDA and 90 mL of CCl_4 were mixed for 12 hours. The mixture was then refluxed at 90˚C in the presence of nitrogen for 6 hours. As a result, black viscous liquid was formed. The liquid was vacuum dried at 120˚ C for 24 hours. After grinding the nanoparticles, calcination was done at 600˚C for 5 hours in nitrogen atmosphere. The black lustrous material formed, called native CN_x nanoparticles, was washed several times with ethanol and then dried at 100˚C.

2.3. Electrospinning

For electrospinning of PVA alone, 3 mL of homogenous solution of 8 % (w/v) PVA was prepared in water. For CN_x/PVA nanofiber system, firstly 0.15 g native CN_x nanoparticles were ultrasonicated in 3 mL water (5 % w/v) for 30 minutes at room temperature. PVA (0.24 g) was added to the CN_x nanoparticles/water dispersion such that 5:8 (wt/wt) ratio of CN_x to PVA is formed. The ratio of 5:8 was chosen for electrospinning because 5 wt% CN_x nanoparticles (active species for ORR) saturates the CN_x nanoparticles/water dispersion and minimum 8 wt% PVA content is necessary to prepare stable, uniform nanofibers. Electrospinning (Super ES-2, E-Spin Nanotech Pvt. Ltd., India) of homogenous solutions was carried out using an infusion syringe pump with a flat tip needle (internal diameter = 0.9 mm) as the spinning head and 50 kV dual polarity high-voltage power supply (Gamma HV). Syringe pump was used to control the flow rate, whereas the high voltage supply was used to charge the needle and the collector. A 15 cm x 15 cm steel plate was used as collector, which was connected to the high voltage supply. Circular glassy carbon electrode was placed on the steel plate for collection of nanofibers for voltammetry. Small amount of Nafion dispersion

was added to improve proton conductivity. Syringe pump was operated at a flow rate of 0.5 mL hr^{-1}. Electrospinning was carried out at a voltage of 10 kV and 30 kV for PVA and CN_x/PVA solutions, respectively. Distance between needle and the collector was kept at 10 cm. The temperature and relative humidity was maintained at 25˚C, 50% RH for all the experiments.

2.4. Physical Characterization

Surface morphology, particle size and diameter of the nanofibers were analysed using SEM, (EVO 50, Zeiss UK electron microscope) and TEM, (FEI Technai G2 20 electron microscope). FTIR study (Bruker Vertex 70v) was carried out to understand the bond structure in the CN_x nanoparticles. X-ray photoelectron spectroscopy (XPS) (Axis His-165 Ultra, Kratos Analytical; Shimadzu, Kyoto, Japan) was carried out to study the characteristic absorption peaks of the samples to confirm the presence of CN_x in the nanofibers. XPS was carried out under a basic pressure of 1.7×10^{-8} Torr, and anode mono-Al with pass energy of 40 (survey scan) was used as X-ray source. Raman spectroscopy (LabRam HR Ar-ion laser 514 nm, Jobin-Yvon, Longjumeau, France) was carried out for native CN_x nanoparticles, CN_x/PVA nanofibers and PVA nanofibers to further confirm the presence of CN_x nanoparticles in the CN_x/PVA nanofibers.

2.5. Working electrode preparation

Working electrodes were prepared using CN_x/PVA nanofibers, PVA nanofibers, native CN_x nanoparticles and Pt/C separately as catalyst material. 20 mg of catalyst was ultrasonicated in solution of 4 mL ethanol and 40 µL Nafion® dispersion for 1 hr. 4 µL of the prepared catalyst ink (for CN_x/PVA nanofibers, native CN_x nanoparticles and PVA nanofibers) was then carefully deposited on circular glassy carbon electrode of 1.6 mm diameter. For Pt/C, 2.4 µL of the catalyst ink was used. In order to understand the ORR catalytic activity of as prepared CN_x/PVA nanofibers, glassy carbon electrode was placed directly on the steel collector during electrospinning. Such CN_x/PVA nanofibers is denoted as CN_x/PVA nanofibers (as prepared) in the study. CN_x/PVA nanofibers coated glassy carbon electrode was also used for *in-situ* FTIR studies, coupled with cyclic voltammetry. For RRDE, CN_x/PVA nanofibers and Pt/C were coated on the disk electrode by preparing catalyst ink.

2.6. Electrochemical characterization for oxygen reduction reaction

Three-electrode cell assembly connected to potentiostat-galvanostat (PGSTAT30, AUTOLAB) was used for cyclic voltammetry (CV) and linear sweep voltammetry (LSV) studies. Ag/AgCl (in saturated KCl) electrode and Pt wire were used as reference and counter electrode respectively. All potential values mentioned are relative to reversible hydrogen

electrode (RHE). The electro-catalyst coated glassy carbon electrode was used as the working electrode with H_2SO_4 (0.5 M) as the electrolyte. CV was carried out on bare glassy carbon electrode for reference. Voltammetry study was carried out in oxygen purged 0.5 M H_2SO_4 solution for CN_x/PVA nanofibers to determine the onset potential and peak current densities. Oxygen reduction reaction (ORR) was studied on prepared native CN_x nanoparticles, CN_x/PVA nanofibers, CN_x/PVA nanofibers (as prepared), PVA nanofibers and Pt/C (40:60 % by weight) catalysts using LSV technique ranging from 1 V to 0.4 V in 0.5 M H_2SO_4 solution and at a scan rate of 20 mV s^{-1}. For native CN_x nanoparticles, PVA nanofibers and CN_x/PVA nanofibers catalyst loading of 1 mg cm^{-2} was used implying that CN_x loading is 385 µg cm^{-2} (5:8) in CN_x/PVA nanofibers. For Pt/C, catalyst loading of 600 µg cm^{-2} was used. ORR mechanism was analysed using rotating ring disk electrode (RRDE) voltammetry and *in-situ* FTIR study combined with cyclic voltammetry. RRDE study was performed using glassy carbon electrode as the disk electrode and platinum ring electrode. The disk electrode potential was swept from 0.8V to 0.2V. The ring potential was maintained at 1.2 V throughout the electrochemical measurements in order to oxidize hydrogen peroxide produced via 2-electron pathway. RRDE of CN_x/PVA nanofibers was carried out for ORR at rotation speeds of 0, 600, 900, 1600 and 2500 RPMs. RRDE of Pt/C was carried out for ORR at 1600 RPM for comparison. *In-situ* FTIR study combined with LSV was conducted on CN_x/PVA nanofibers and the corresponding spectra were plotted at different potentials. *In-situ* FTIR studies with voltammetry was conducted over 6000 repetitions to analyse the catalytic activity of CN_x/PVA nanofibers over a period of time. FTIR spectrum, corresponding to 5^{th}, 1000^{th}, 2000^{th}, 3000^{th} and 5000^{th} repetition was recorded at 0.7 V. For both RRDE study and *in-situ* FTIR with LSV studies, Ag/AgCl (in saturated KCl), Pt wire and oxygen purged 0.5 M H_2SO_4 solution were used as reference electrode, counter electrode and electrolyte, respectively. TEM was carried out of CN_x/PVA nanofibers after dispersing it in IPA before voltammetry, and after 2000 and 5000 repetitions of LSV for ORR to further understand the catalyst behaviour during voltammetry.

2.7. Scanning electrochemical microscopy

In order to understand the electron conductivity of CN_x/PVA nanofibers, scanning electrochemical microscopy (SECM) was carried out using Sensolytics SECM setup attached to PGSTAT30, Autolab. SECM was operated under feedback mode. For conducting SECM, CN_x/PVA nanofibers were coated on carbon paper. SECM was also carried out for the base material (carbon paper) for comparison. Pt microelectrode (25 µm) was used as working electrode, Pt foil as counter electrode, Ag/AgCl (sat KCl) as reference electrode and oxygen

saturated 0.5 M H_2SO_4 solution as electrolyte. Voltage of 0.5 V was applied at Pt microelectrode and current generated was observed.

3. Results and discussions

3.1. SEM and TEM

TEM micrograph of the native CN_x nanoparticles is shown in Figure 1(a). The figure indicates that nanoparticles are formed in irregular shapes with size of around 20 nm. The CN_x nanoparticles agglomerates quickly as shown in Figure 1(a). Figure 1(b) shows SEM micrograph of the CN_x/PVA nanofibers at a lower magnification indicating the formation of dense, multi-layered nanofibers. TEM micrographs of CN_x/PVA nanofibers shown in Figures 1 (c), 1 (d) and 1 (e) confirm the presence of CN_x nanoparticles in the nanofibers. In most of the cases it is seen that CN_x nanoparticles are bulging out from nanofibre (figure 1 (c)) possibly allowing contact with glassy carbon electrode or carbon paper. Some times CN_x nano partclies are completely embedded inside PVA nanofibers (figure 1 (d)) preventing contact with electrode. Overall diameter of CN_x/PVA nanofibers lies in the range of 20 nm to 320 nm. The large range of size is attributed to non-uniform dispersion of conducting CN_x nanoparticles in the PVA solution. The region with more concentration of CN_x nanoparticles have smaller size nanofibers due to high electrostatic forces. High electrostatic force dominates surface tension force leading to breaking of nanofibers at some points. It is seen in figure 1 (e) that CN_x/PVA nanofibers are parallely aligned entrapping CN_x nanoparticles, which prevents its agglomeration and at tahe same time allows contact with elecrtode. When spread on to the glassy carbon electrode by Nafion dispersion CN_x/PVA nanofibre allows both electronic and proton conductivity. If the CN_x nano powder completely embedded in PVA nanofibre, maintaining connectivity for proton and electron transfer would not be possible.

3.2 FTIR

FTIR spectrum of native CN_x nanoparticles is shown in Figure 2. The three major bands centred at around 1100, 1626 and 3418 cm^{-1} confirm the presence of aromatic C-N single bond stretching mode, deformation modes and stretching mode of N-H groups respectively[30]. Moreover, the absence of C≡N is confirmed as no peak at 2200 cm^{-1} is found. The bands around 2922 and 2854 cm^{-1} correspond to terminal CH_3 group. The band around 1384 cm^{-1} and the shoulder around 1224 cm^{-1} correspond to sp^3 C-C bond[30]. The data further confirms the presence of nitrogen in pyridinic and pyrrolic form. FTIR spectra of CN_x/PVA show some notable differences from PVA spectra. There is a major band in CN_x/PVA nanofibers at around 1100 cm^{-1} as in the spectrum of native CN_x nanoparticles, which is expected due to

the presence of C-N single bond stretching mode of CN_x in the nanofibers. Shifting of peak from 3430 cm^{-1} in PVA (due to OH stretch mode in alcohols) and 3420 cm^{-1} in native CN_x nanoparticles to 3310 cm^{-1} in CN_x/PVA nanofibers shows that there are some interactions between the CN_x nanoparticles and PVA leading to certain structural modifications, which may be responsible for enhanced ORR activity and conductivity. The band at 1650 cm^{-1} in CN_x/PVA nanofibers confirms the presence of N-H bending mode, as observed in XPS. Since there is no significant change in the percentage of pyridine form of N in CN_x/PVA nanofibers than in native CN_x nanoparticles (as confirmed in XPS), it is inferred that a percentage of pyrrolic form of N is converted to amino N. This is possible as electrospinning of the solution with nanoparticles required high voltage (30 kV) and some percentage of pyrrolic N of CN_x absorbs this energy and gets converted to amino N. Since amino N contributes to the ORR and pyrrolic N does not[31], the conversion to amino N contributes to increase in ORR activity with the CN_x/PVA nanofibers. The band at 1730 cm^{-1} corresponds to C=O in aldehydes, due to modification in PVA structure. It can be inferred that the alcohol in the PVA gets converted to aldehydes. The resulting H species, along with the high energy due to the electrospinning process, aids in the conversion of pyrrole group to the more active amino group.

3.3 XPS

X-ray photoelectron spectroscopy (XPS) for native CN_x nanoparticles and CN_x/PVA nanofibers are shown in Figure 3. C 1s peak of both, nanoparticles and nanofibers corresponding to the binding energy of 284.6 eV and 285.7 eV, matches with the binding energy of pure graphitic sites and sp^2 C atoms bonded to N inside the aromatic structure respectively. The small peak at 288.8 eV corresponds to sp^2 hybridised carbon in the aromatic ring attached to NH_2 group[30]. N 1s peak analysis for the CN_x nanoparticles shows the presence of peaks at 400.7 eV and 398.9 eV, which correspond to pyrrolic N and pyridinic N, respectively[31]. Nitrogen was observed to be in very little quantity in nanofibers (2%) as compared to the nanoparticles (29%). This underestimation of nitrogen content is because of the huge carbon content present in both CN_x and PVA[12]. A new peak for nanofibers at 399.7 eV is noticed, which corresponds to amino N. Small amount of pyrrolic N, being least stable[31], gets converted to amino N on application of high potential during electrospinning, as explained in FTIR. The percentage of pyridinic N, mainly responsible for ORR, in CN_x/PVA nanofibers (68%) is similar to that in native CN_x nanoparticles (65%). It is worth noticing that in spite of the fact that nitrogen content is reduced considerably in nanofibers, the activity of the nanofibers has increased for ORR, which is attributed to the increase in surface area per

unit volume of the CN_x nanoparticles in the nanofibers as compared to its agglomerate form. The conversion of inactive pyrrolic N to active amino N also contributes to increase in the ORR activity.

3.4 Raman spectroscopy

Figure 4 shows the Raman spectra for native CN_x nanoparticles, CN_x/PVA nanofibers and PVA nanofibers under the same conditions during measurement. The D and G bands around 1350 and 1590 cm^{-1} are present in both native CN_x nanoparticles and CN_x/PVA nanofiibers. G band corresponds to sp^3 hybridised (graphitic) carbon and D band corresponds to structural defects at the edges of sp^2 hybridised carbon (attributed to pyridinic N in the structure), which further confirms the results of XPS analysis. The intensity ratio of D and G bands (I_D/I_G) is calculated to determine the extent of defects induced as a result of the presence of pyridinic N in both native CN_x nanoparticles and CN_x/PVA nanofibers[31]. For both the cases, I_D/I_G ratio is calculated to be 0.3, which shows that pyridinic character of CN_x nanoparticles survived under the high voltage and electrostatic force during electrospinning process, as confirmed by XPS as well. The decrease in intensities of the peaks in the nanofibers is attributed to the underestimation of the CN_x nanoparticles due to higher PVA content in the nanofibers. It may be noted that no significant peak is observed in the Raman spectrum of PVA nanofibers in the range 1300 to 1700 cm^{-1}.

3.5. Voltammetry

Figure 5 (a) and (b) shows linear sweep voltammetry plots for native CN_x nanoparticles, CN_x/PVA nanofibers, CN_x/PVA nanofibers (as prepared), PVA nanofibers, Pt/C and bare glassy carbon electrode. The potential window for CV is shown from 0.2 V to 1.2 V because no characteristic peak was observed by extending the potential range beyond 1.2 V. The plots reveal significant improvement in electrocatalytic activity of CN_x nanoparticles dispersed in PVA nanofibers as compared to its native form. The onset potentials for the catalysts, determined from the plots, where the slope changes prior to the reduction peaks, and peak current densities are indicated in table 1. Since PVA does not exhibit any ORR activity, as shown in expanded portion of I of figure 5(a) in figure 5(b), the catalytic activity of CN_x/PVA nanofibers is attributed to active CN_x nanoparticles. The observed onset potential of 0.88 V and peak current density of 5.48 mA cm^{-2} for CN_x/PVA nanofibers is enhanced as compared to onset potential (0.75 V) and peak current density (0.12 mA cm^{-2}) of CN_x nanoparticles in its native form. Enhanced onset potential substantiates that CN_x/PVA nanofibers offer less resistance to ORR. The CN_x/PVA nanofibers exhibit similar peak current density for ORR when employed as prepared and as catalyst ink. However, CN_x/PVA

nanofibers (catalyst ink) gives a broad voltage-current density peak, whereas CN_x/PVA nanofibers (as prepared) gives relatively sharper peak. The catalytic activity of CN_x/PVA nanofibers is comparable to Pt/C catalyst (onset potential: 0.97 V and peak current density: 6.41 mA cm^{-2}). The improvement in mass activity 16 A g^{-1} of CN_x nanoparticles in CN_x/PVA nanofibers as compared to 0.12 A g^{-1} in native form is attributed to the increased number of active sites in the entrapped nanofibers due to dispersion of CN_x nanoparticles in PVA nanofibers as compared to the agglomerated native CN_x nanoparticles and conversion of some of the pyrrole N to amino N during electrospinning and structural modification of CN_x/PVA interface. The ORR activity of CN_x/PVA nanofibers is improved as compared to previously reported bulk CN_x supported on carbon black (Onset potential: 0.76 V and peak current density of 2.21 mA cm^{-2})[14] and bulk CN_x pyrolysed at 1000 °C (onset potential 0.85 V)[12].

The disk current and ring current plots for RRDE experiment of CN_x/PVA nanofibers for ORR at 0, 600, 900, 1600 and 2500 RPMs are shown in Figure 6 (a) and 6 (b). The disk current and ring current plots for RRDE experiment of Pt/C for ORR at 1600 RPM is also shown in figure 6 (a) and (b). It is seen that ORR activity of CN_x/PVA nanofibers is comparable to Pt/C. The number of electrons (n) transferred for CN_x/PVA nanofibers is calculated from the formula for ORR mechanism[12]:

$$n = \frac{4I_d}{I_d + \frac{I_r}{N}} \qquad (1)$$

Where, n is the number of electrons transferred, I_r is the ring current (A), I_d is the disk current (A) and N is the collection efficiency of the ring (0.424). The values of n in the potential range of 0.2 to 0.6 are plotted for CN_x nanoparticles and CN_x/PVA nanofibers (figure 6 (c)). Average values of n equals to 3.5 and 3.7 are obtained for CN_x nanoparticles and CN_x/PVA nanofibers, respectively. It indicates that ORR on CN_x nanoparticles predominantly takes place via highly efficient 4-electron pathway. The 'n' value was further confirmed using Koutecky-Levich equation[31]:

$$\frac{1}{I_d} = \frac{1}{I_k} + \frac{1}{B\omega^{1/2}} \qquad (2)$$

$$B = 0.2\, n\, F\, A\, C_{O_2}\, D_{O_2}{}^{2/3}\, \upsilon^{-1/6} \qquad (3)$$

Where, I_k is the kinetic current, ω is the rotation per minute, n is the number of electrons transferred, F is the Faraday's constant (96500), A is the electrode area (0.1256 cm^2), C_{O_2} is the concentration of O_2 in 0.5 M sulphuric acid ($1.1X10^{-6}$ mol cm^{-3}), D_{O_2} is the diffusion

coefficient ($1.4X10^{-5}$ cm^2 s^{-1}), υ is the kinematic viscosity (0.01 cm s^{-1}). The Koutecky-Levich (I_d^{-1} vs $\omega^{-1/2}$) plots at different potentials shown in figure 6 (d) exhibit close linearity. The slopes of the lines closely match with that of the reference plot for n = 4 and n value of 3.7 is obtained, which further confirms the dominance of 4-electron pathway mechanism. Hydrogen peroxide yield is calculated from RRDE data for CN_x/PVA nanofibers from the formula[32], $\%H_2O_2 = 200\frac{\frac{I_r}{N}}{I_d+\frac{I_r}{N}}$, Hydrogen peroxide yield is calculated to be ~22 %. Same percentage of hydrogen peroxide yield is previously reported[12] for bulk CN_x pyrolised at 1000 ºC. The H_2O_2 formation can be attributed to the ORR occurring on amino N (21% of present N in CN_x/PVA nanofibers) sites present in CN_x/PVA nanofibers as it has already been established in the literature that ORR on amino N sites takes place via combination of 2-electron and 4-electron reactions[33]. ORR on pyridinic N (68 % of present N in CN_x/PVA nanofibers) sites occur via 4-electron pathway towards water formation with little or no hydrogen peroxide formation[31].

Figure 7 (a) shows the *in-situ* FTIR peaks combined with cyclic voltammetry (figure 7 (b)). Cyclic voltammetry shows quinone-hydroquinone type redox couple which does not take part in ORR, confirmed by its presence in nitrogen atmosphere[14]. CV reveals that ORR in oxygen atmosphere initiates at 0.88 V and it continues till the reduction peak of the quinone-hydroquinone type redox couple is reached, depicted by increase in current density at peak potential in oxygen atmosphere as compared to nitrogen atmosphere. The same is confirmed by *in-situ* FTIR results as shown in three bands (Figures 7(c)-(e)). The band X (3410 cm^{-1}) in figures 7(c) is attributed to water υ (OH) band formed as a result of end product of ORR[33]. The band Y (2590 cm^{-1}) and Z (1980 cm^{-1}) in figure 7(d) and (e) are attributed to hydroquinone and quinone type structure associated with reduction and oxidation peaks of the redox couple respectively. The band X is observed to increase with decrease in potential till 0.5 V, confirming occurrence of ORR throughout the range. A slight decrease in band X observed between 0.9 V and 0.8 V implies the initiation of ORR. If the water formation had not started, the dip in the peak would have been significant, as can be observed in band Y and Z in the potential region 0.9 V to 0.8 V, where redox couple is not initiated yet. The band Y peak is slightly shifted in the range of 0.8 V to 0.7 V, attributed to the significant changes in bond behaviour due to simultaneous occurrence of ORR and initiation of reduction of quinone type structure at the electrode. The band Y peak increases while reducing potential

further to 0.5 V, corresponding to reduction peak in CV. Similarly, the band Z peak increases with decrease in potential in the range 0.8 V to 0.5 V corresponding to oxidation peak in CV.

In order to understand the ORR activity over a period of time, CN_x/PVA nanofibers were subjected to 6000 repetitions of the reduction under *in-situ* FTIR and voltammetry studies. ORR linear sweep voltammograms at different LSV repetitions is shown in figure 8 (a). Corresponding FTIR spectra at 0.7 V at different LSV repetitions are shown in figure 8 (b). It is noticed that ORR activity of CN_x/PVA nanofibers improves with increasing number of repetitions. However the ORR activity becomes stable after 5000 repetitions. There is no appreciable change in voltammogram is noticed at 6000^{th} repetition. In FTIR, major changes in four peaks are studied, namely, 3410 cm^{-1} (K), 2590 cm^{-1} (L), 1980 cm^{-1} (M) and 2350 cm^{-1} (N).

Initially, ORR and hydroquinone-quinone type redox reaction is initiated as observed from the presence of bands K, L and M during initial 5 repetitions. During 5 to 1000 LSV repetitions, sharp increase in band L and band M suggests formation of hydroquinone and quinone type structures subjugating the water band (K) peak at the electrode. During 1000 to 2000 LSV repetitions, no significant change in bands L and M are observed. However improvement in reduction peaks suggest that hydroquinone-quinone type redox reactions are dominant during this period. The reversible nature of the reaction contributes to no change in peaks in bands L and M. In the LSV repetitions 2000 to 3000, the ORR reaches a steady state with a slight improvement in L and M bands. It may be noticed water formation due to ORR begin to dominate resulting in sharp increase in band K peak. After 3000 LSV repetitions, ORR dominates at the electrode resulting in decrease in bands L and M peaks and an increase in band K peak. The continuous decrease of band N, assigned to evolution of CO_2 in the electrolyte surrounding the electrode, which may be due to the degeneration of glassy carbon electrode or PVA. This may require further investigation. The overall dominance of ORR after 5000 LSV repetitions suggests CN_x/PVA catalytically stable for ORR.

In order to understand the possible reason for the ORR catalytic activity of CN_x/PVA nanofibers, TEM was carried out for CN_x/PVA nanofibers after dispersing it in isopropyl alcohol (IPA) before ORR voltammetry (figure 9 (a)), after 2000 repetitions of LSV (figure 9 (b)) and after 5000 repetitions of LSV (figure 9 (c)). It is seen in figure 9 (a) that CN_x

nanoparticles are present on the surface and bulk of the nanofiber. CN_x/PVA nanofiber becomes lighter in nature, as seen in figure 9 (b), after 2000 repetitions of LSV. PVA may be dissloving out of the fiber exposing CN_x nanoparticle on the surface of the fiber. After 5000 repetitions of LSV, it can be noticed that the PVA nanofibers have disintegrated (figure 9 (c)) but CN_x nanoparticles still remain attached to disintegrated form of PVA with the formation of agglomerates. Retention of CN_x nanoparticles on the glassy carbon electrode or carbon paper is attributed to the presence of Nafion dispersion and binding property of PVA, although not present in nanofiber form.

In order to understand the electron conductivity of CN_x/PVA nanofibers, SECM is carried out for CN_x/PVA nanofibers coated on carbon aper and uncoated carbon paper. Increased current generated for CN_x/PVA nanofibers as compared to carbon paper at the microelectrode during the approach curve (figure 10 (a)) confirms the conductive nature of CN_x/PVA nanofibers. SECM plot of current variation with electrode area surface (XY) keeping height (Z) constant is plotted (figure 10 (b)). Z is the electrochemical active region of the CN_x/PVA nanofibers coated and uncoated carbon paper very close to the surface, decided by the approach curve experiment. It is seen that an increase in current for CN_x/PVA nanofibers is observed as compared to uncoated carbon paper, which further confirms the conductive nature of CN_x/PVA nanofibers.

4. Conclusion

Electrocatalytic activity of CN_x nanoparticles is improved by many folds by dispersing it in PVA nanofibers as compared to its agglomerated native form. PVA nano fibre not only helps in dispersing and entrapping CN_x nano particles, but also responsible for improved ORR activity as shown by XPS and Raman spectra confirming the presence of pyridine N and conversion of small percentage of pyrrole N to active amino N during high voltage application in electrospinning. Improved onset potential and peak current density of CN_x/PVA nanofibers for ORR are observed in voltammetry which is comparable to platinum based catalyst. RRDE studies confirm that CN_x/PVA nanofibre follows 4-electron ORR pathway. Active sites of CN_x/PVA nanofibers is found to be stable on exposing it to 5000 voltammetric repetitions observed under *in-situ* FTIR.

5. Acknowledgement

Authors would like to acknowledge Department of Information Technology, Government of India and RCUK-DST for funding the project.

References

1 S. Basu (Ed.), *Recent Trends in Fuel Cell Science and Technology*, Springer, New York, 2007.

2 N. M. Markovic, H. a Gasteiger, B. N. Grgur and P. N. Ross, *J. Electroanal. Chem.*, 1999, **467**, 157–163.

3 H. Naohara, S. Ye and K. Uosaki, *Electrochim. Acta*, 2000, **45**, 3305–3309.

4 L. Zhang and Z. Xia, *J. Phys. Chem. C*, 2011, **115**, 11170–11176.

5 Y. Li, W. Zhou, H. Wang, L. Xie, Y. Liang, F. Wei, J.-C. Idrobo, S. J. Pennycook and H. Dai, *Nat. Nanotechnol.*, 2012, **7**, 394–400.

6 J. Liu, D. Takeshi, D. Orejon, K. Sasaki and S. M. Lyth, *J. Electrochem. Soc.*, 2014, **161**, F544–F550.

7 R. Wang, T. Zhou, H. Li, H. Wang, H. Feng, J. Goh and S. Ji, *J. Power Sources*, 2014, **261**, 238–244.

8 D. Singh, J. Tian, K. Mamtani, J. King, J. T. Miller and U. S. Ozkan, *J. Catal.*, 2014, **317**, 30–43.

9 V. Nallathambi, N. Leonard, R. Kothandaraman and S. C. Barton, *Electrochem. Solid-State Lett.*, 2011, **14**, B55–B58.

10 H. Li, H. Liu, Z. Jong, W. Qu, D. Geng, X. Sun and H. Wang, *Int. J. Hydrogen Energy*, 2011, **36**, 2258–2265.

11 S. Chen, J. Bi, Y. Zhao, L. Yang, C. Zhang, Y. Ma, Q. Wu, X. Wang and Z. Hu, *Adv. Mater.*, 2012, **24**, 5593–5597.

12 S. M. Lyth, Y. Nabae, N. M. Islam, S. Kuroki, M. Kakimoto and S. Miyata, *J. Electrochem. Soc.*, 2011, **158**, B194–B201.

13 Y. Zheng, J. Liu, J. Liang, M. Jaroniec and S. Z. Qiao, *Energy Environ. Sci.*, 2012, **5**, 6717–6731.

14 S. M. Lyth, Y. Nabae, S. Moriya, S. Kuroki, M. A. Kakimoto, J. I. Ozaki and S. Miyata, *J. Phys. Chem. C*, 2009, **113**, 20148–20151.

15 Y. Miyamoto, M. L. Cohen and S. G. Louie, *Solid State Commun.*, 1997, **102**, 605–608.

16 M. Terrones, H. Terrones, N. Grobert, W. K. Hsu, Y. Q. Zhu, J. P. Hare, H. W. Kroto, D. R. M. Walton, P. Kohler-Redlich, M. Ruhle, J. P. Zhang and a K. Cheetham, *Appl. Phys. Lett.*, 1999, **3932**, 25–28.

17 P. K. Panda, *Ceram. Int.*, 2013, **39**, 4523–4527.

18 S. L. Sung, S. H. Tsai, C. H. Tseng, F. K. Chiang, X. W. Liu and H. C. Shih, *Appl. Phys. Lett.*, 1999, **74**, 197–199.

19 M. Terrones, N. Grobert, J. Olivares, J. P. Zhang, H. Terrones, K. Kardatos, W. K. Hsu, J. P. Hare, P. D. Townsend, K. Prassides, A. K. Cheetham, H. W. Kroto and D. R. M. Walton, *Nat.*, 1997, **388**, 52–55.

20 M. Terrones, N. Grobert, J. P. Zhang, H. Terrones, J. Olivares, W. K. Hsu, J. P. Hare, a. K. Cheetham, H. W. Kroto and D. R. M. Walton, *Chem. Phys. Lett.*, 1998, **285**, 299–305.

21 M. Terrones, P. Redlich, N. Grobert, S. Trasobares, W. Hsu, H. Terrones, Y. Zhu, J. P. Hare, C. L. Reeves, A. K. Cheetham, M. Rühle, H. W. Kroto and D. R. M. Walton, *Adv. Mater.*, 1999, **11**, 655–658.

22 C. R. Martin, *Chem. Mater.*, 1996, **8**, 1739–1746.

23 T. Ondarçuhu and C. Joachim, *Europhys. Lett.*, 1998, **42**, 215–220.

24 P. X. Ma and R. Zhang, *J. Biomed. Mater. Res.*, 1999, **46**, 60–72.

25 G. Liu, J. Ding, L. Qiao, A. Guo, B. P. Dymov, J. T. Gleeson, T. Hashimoto and K. Saijo, *Chem. - A Eur. J.*, 1999, **5**, 2740–2749.

26 Z. M. Huang, Y. Z. Zhang, M. Kotaki and S. Ramakrishna, *Compos. Sci. Technol.*, 2003, **63**, 2223–2253.

27 D. H. Reneker and A. L. Yarin, *Polymer (Guildf).*, 2008, **49**, 2387–2425.

28 M. S. Islam and M. R. Karim, *Colloids Surfaces A Physicochem. Eng. Asp.*, 2010, **366**, 135–140.

29 Y. Qiu and L. Gao, *Chem. Commun. (Camb).*, 2003, 2378–2379.

30 A. Vinu, K. Ariga, T. Mori, T. Nakanishi, S. Hishita, D. Golberg and Y. Bando, *Adv. Mater.*, 2005, **17**, 1648–1652.

31 N. Daems, X. Sheng, I. F. J. Vankelecom and P. P. Pescarmona, *J. Mater. Chem. A*, 2014, **2**, 4085–4110.

32 X. Yang, L. Gan, C. Zhu, B. Lou, L. Han, J. Wang and E. Wang, *Chem. Commun.*, 2014, **50**, 234–236.

33 K. Kunimatsu, T. Yoda, D. A. Tryk, H. Uchida and M. Watanabe, *Phys. Chem. Chem. Phys.*, 2010, **12**, 621–629.

Catalyst	Onset potential (V)	Peak current density (mA cm^{-2})
CN_x/PVA nanofibers	0.88	-5.48
Native CN_x nanoparticles	0.75	-0.12
Pt/C	0.97	-6.41

Table 1: Comparison of onset potential and peak current density of CN_x/PVA nanofibers, native CN_x nanoparticles and Pt/C

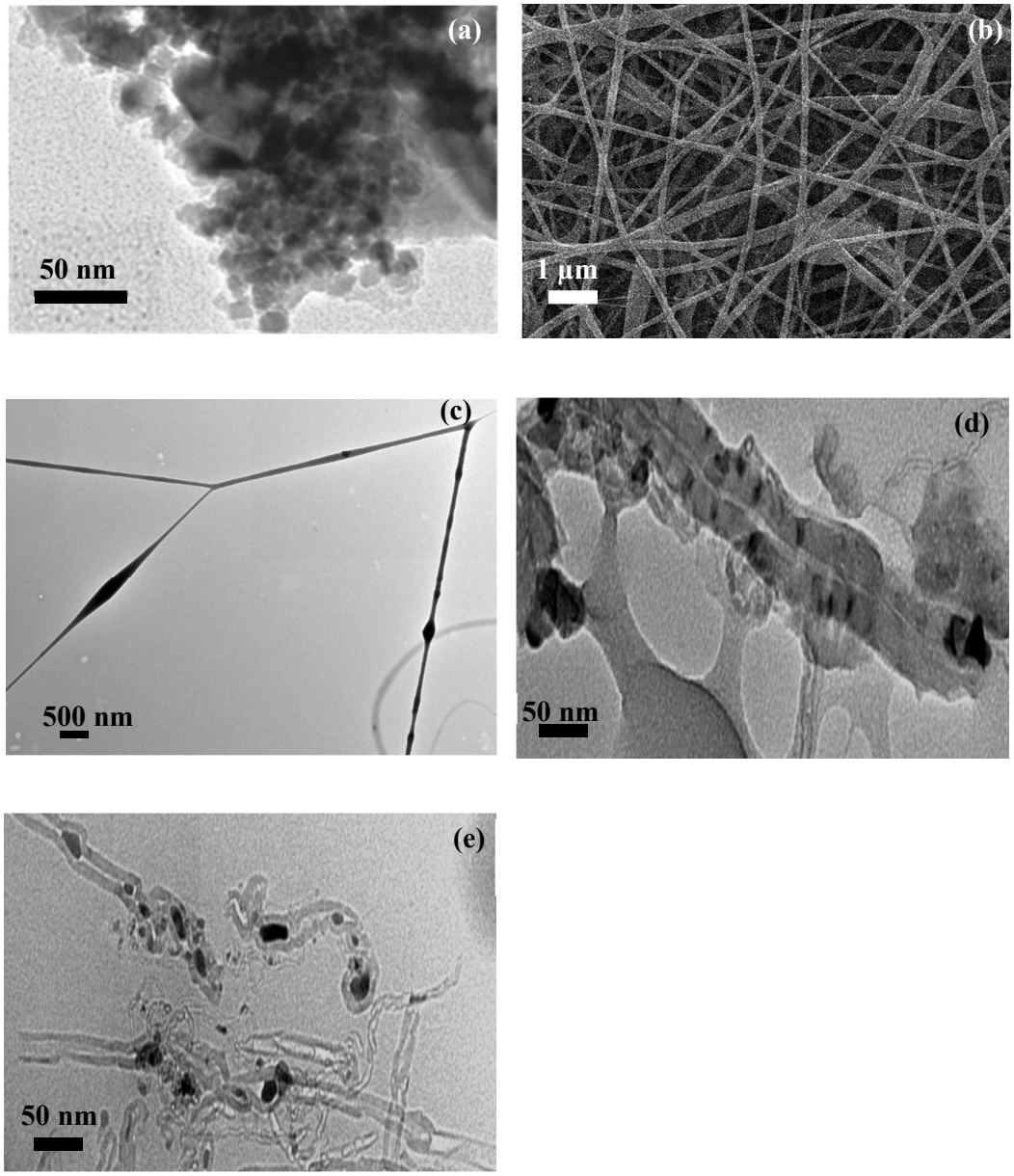

Figure 1: (a) TEM image of native CN_x nanoparticles, (b) SEM image of CN_x/PVA nanofibers (c) TEM image of CN_x/PVA nanofibers showing nanofibers of diameter ~ 150 nm, (d) TEM image of CN_x/PVA nanofibers with CN_x nanoparticles embedded in the CN_x/PVA nanofibers and (e) TEM image of CN_x/PVA nanofibers with CN_x nanoparticles entrapped within two aligned nanofibers

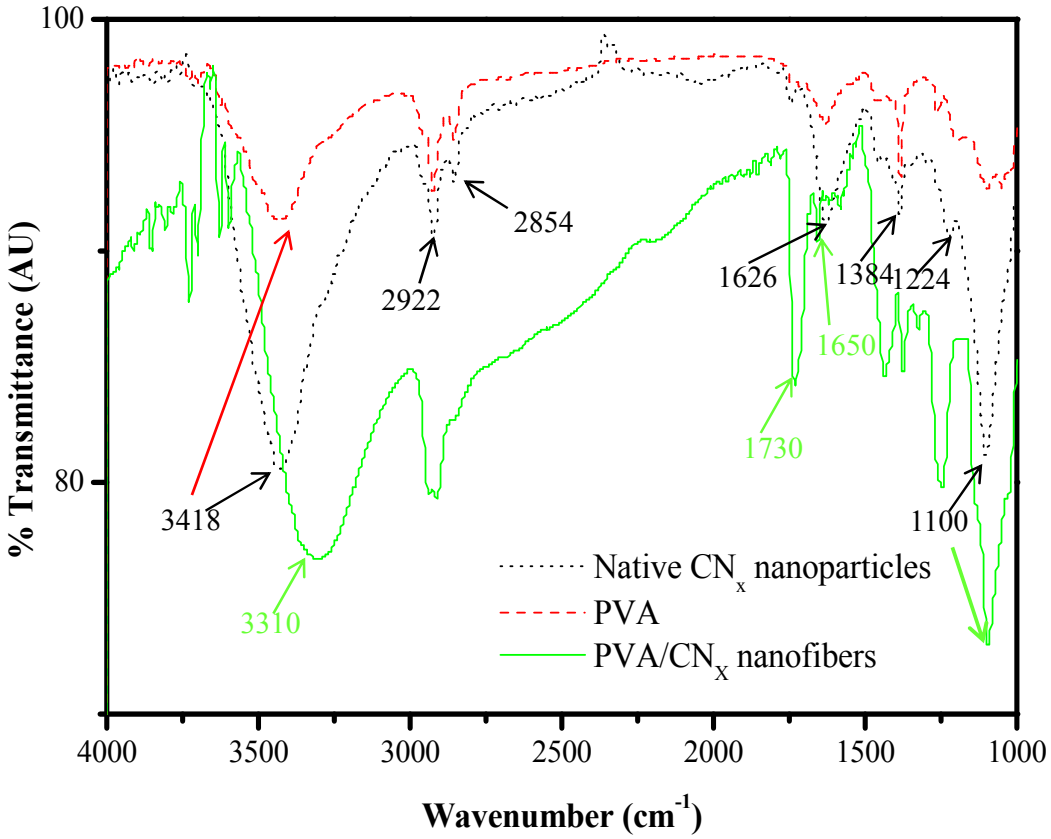

Figure 2: FTIR of native CN_x nanoparticles, PVA nanofibers and CN_x/PVA nanofibers

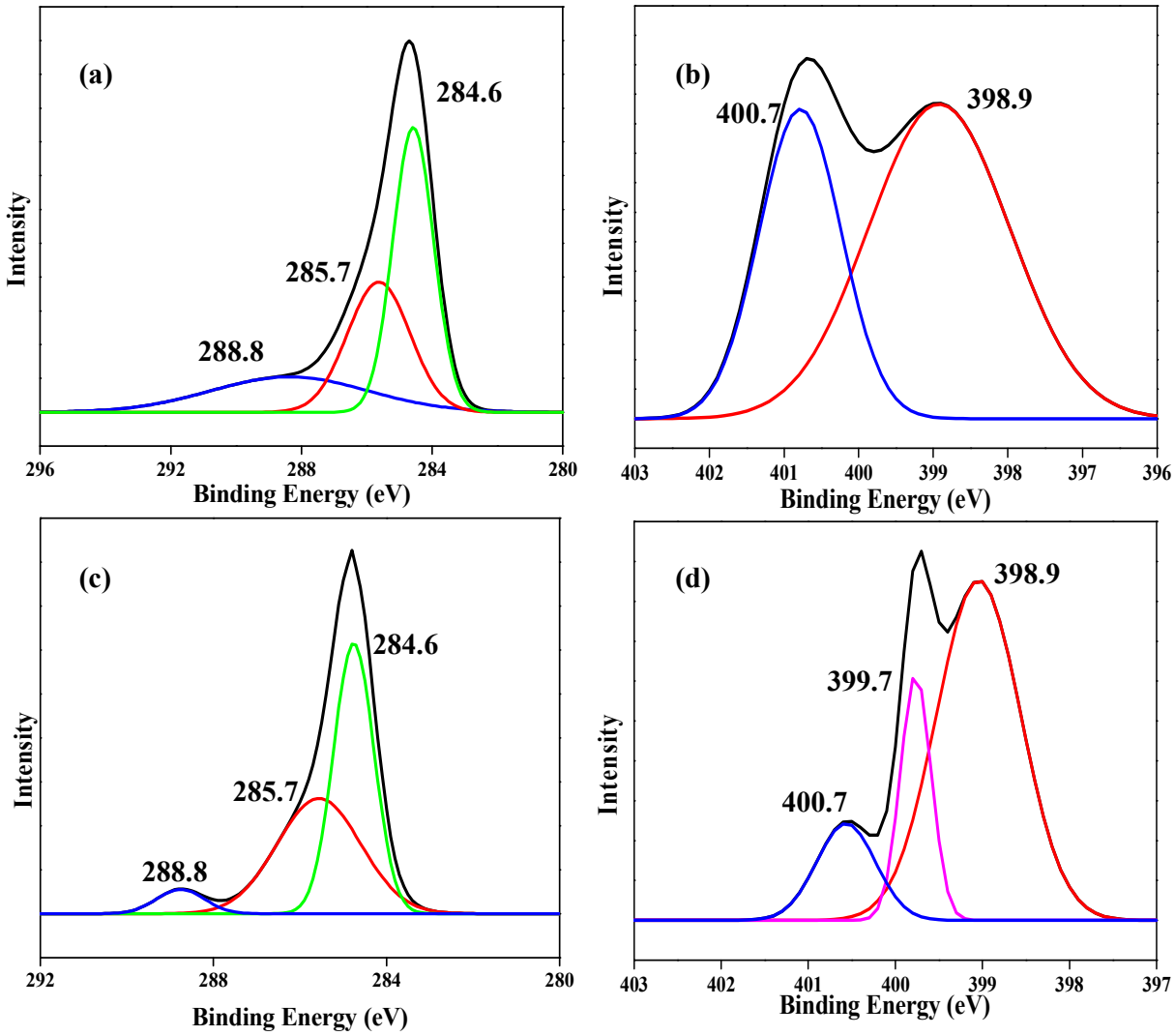

Figure 3: XPS spectra of CN_x nanoparticles for (a) C1s peaks and (b) N1s peaks; XPS spectra of CN_x/PVA nanofibers for (c) C1s and (d) N1s peaks

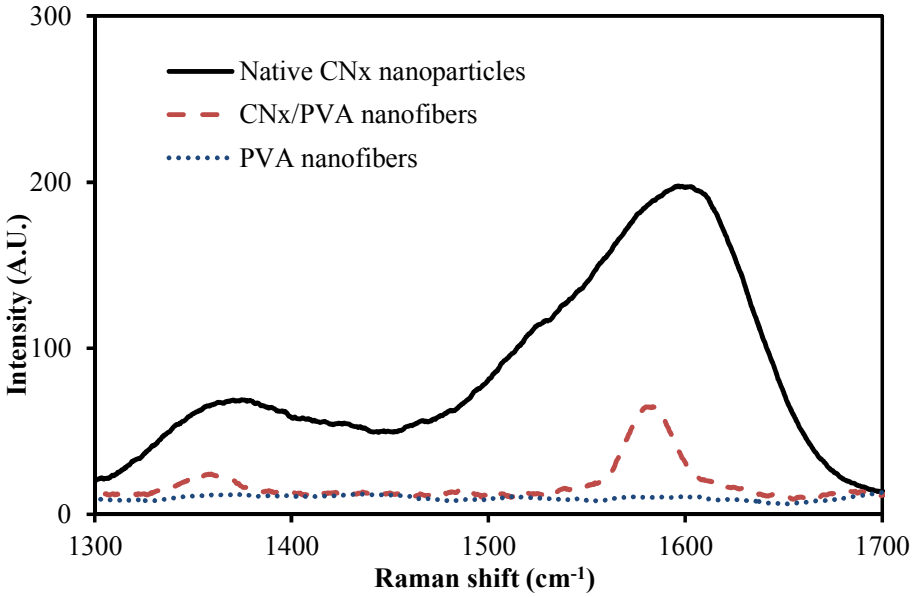

Figure 4: Raman spectra at 514.5 nm wavelength of native CN_x nanoparticles, CN_x/PVA nanofibers and PVA nanofibers

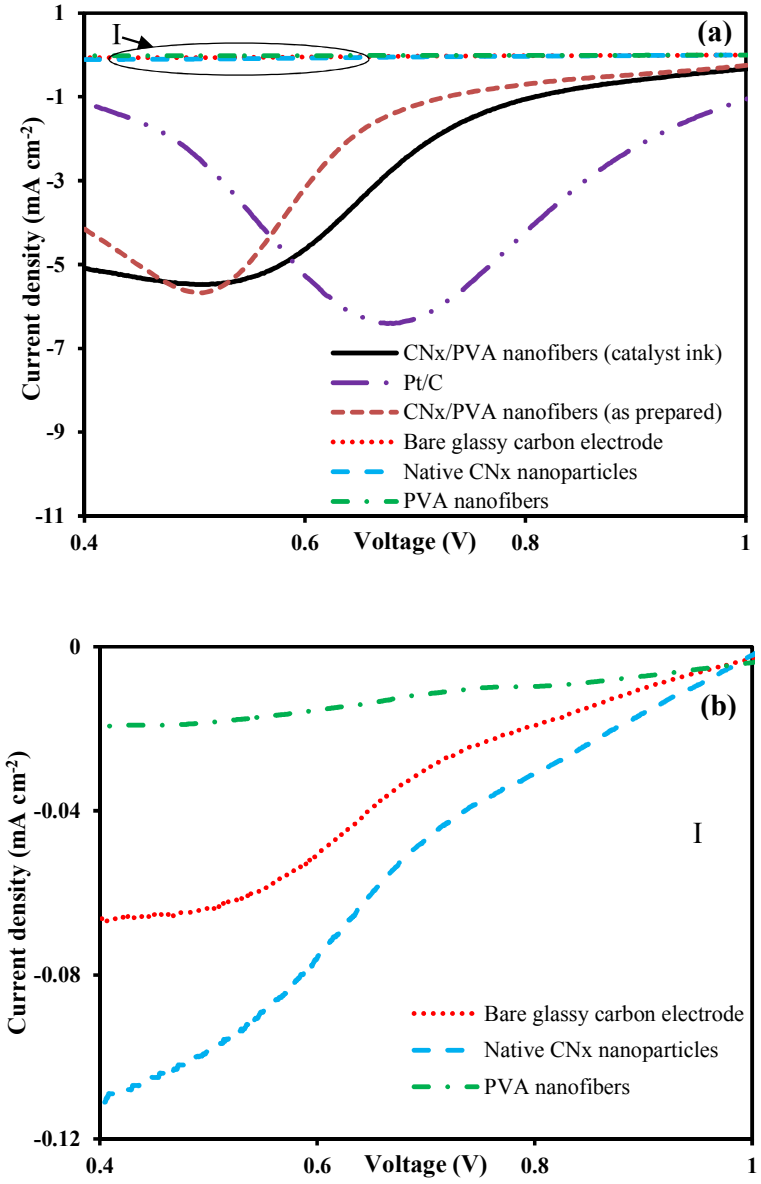

Figure 5: (a) Linear sweep voltammograms of CN_x/PVA nanofibers (prepared through catalyst ink and as prepared), native CN_x nanoparticles, Pt/C, PVA nanofibers and bare glassy carbon electrode in 0.5 M H_2SO_4 solution at scan rate of 20 mV s^{-1} for ORR. (b) Expanded portion (I) of the voltammograms of native CN_x nanoparticles, PVA nanofibers and bare glassy carbon electrode

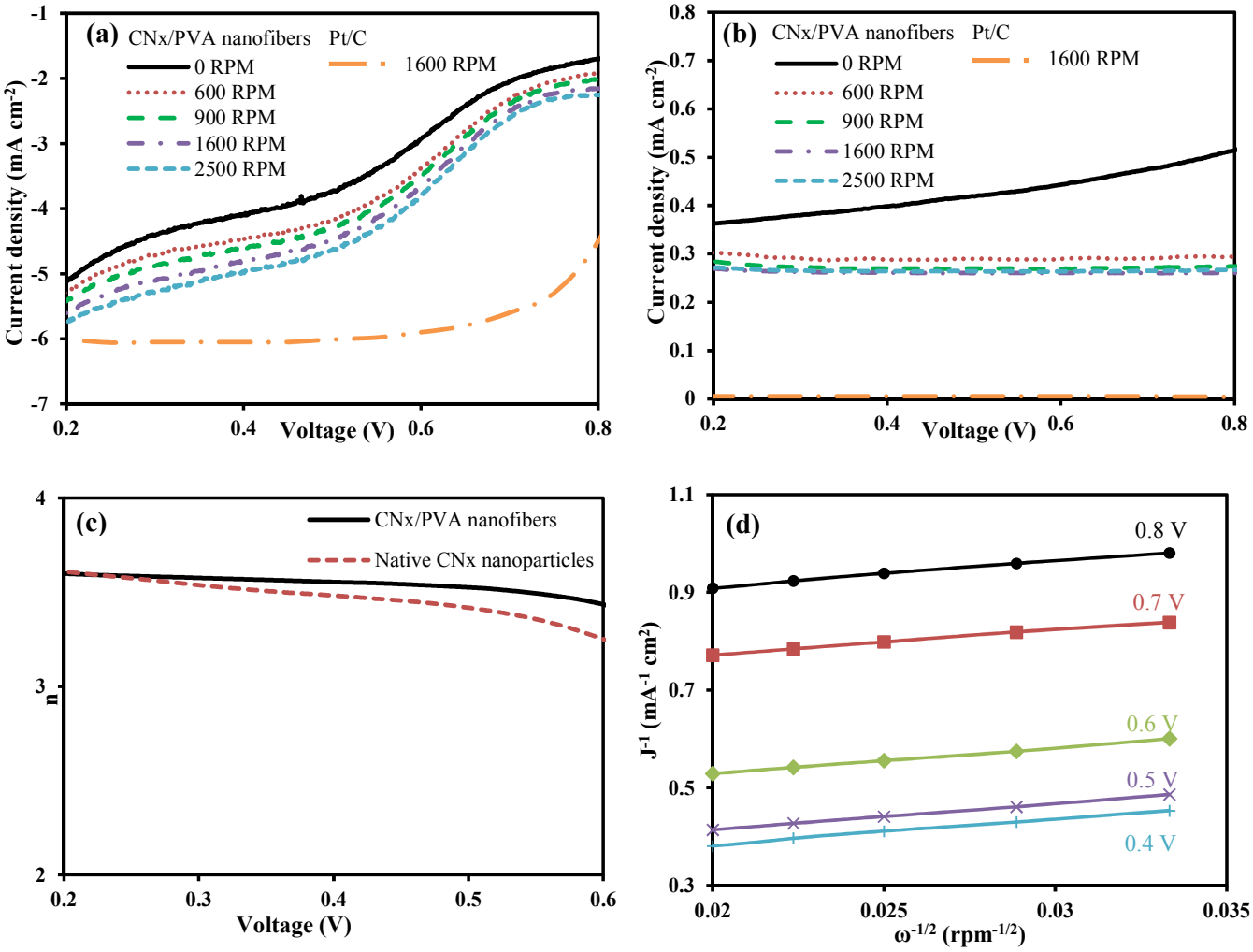

Figure 6: Linear sweep voltammograms of CN_x/PVA nanofibers for ORR showing the variation of current density with rotation speed and that of Pt/C at 1600 RPM on a rotating ring disc glassy carbon electrode in 0.5 M H_2SO_4 solution at scan rate of 20 mV s^{-1}: (a) Disk current; (b) Ring current; (c) number of electrons exchanged versus voltage for CN_x/PVA nanofibers (equation 1) and (d) Koutecky Levich plot for ORR for CN_x/PVA nanofibers (equation 2)

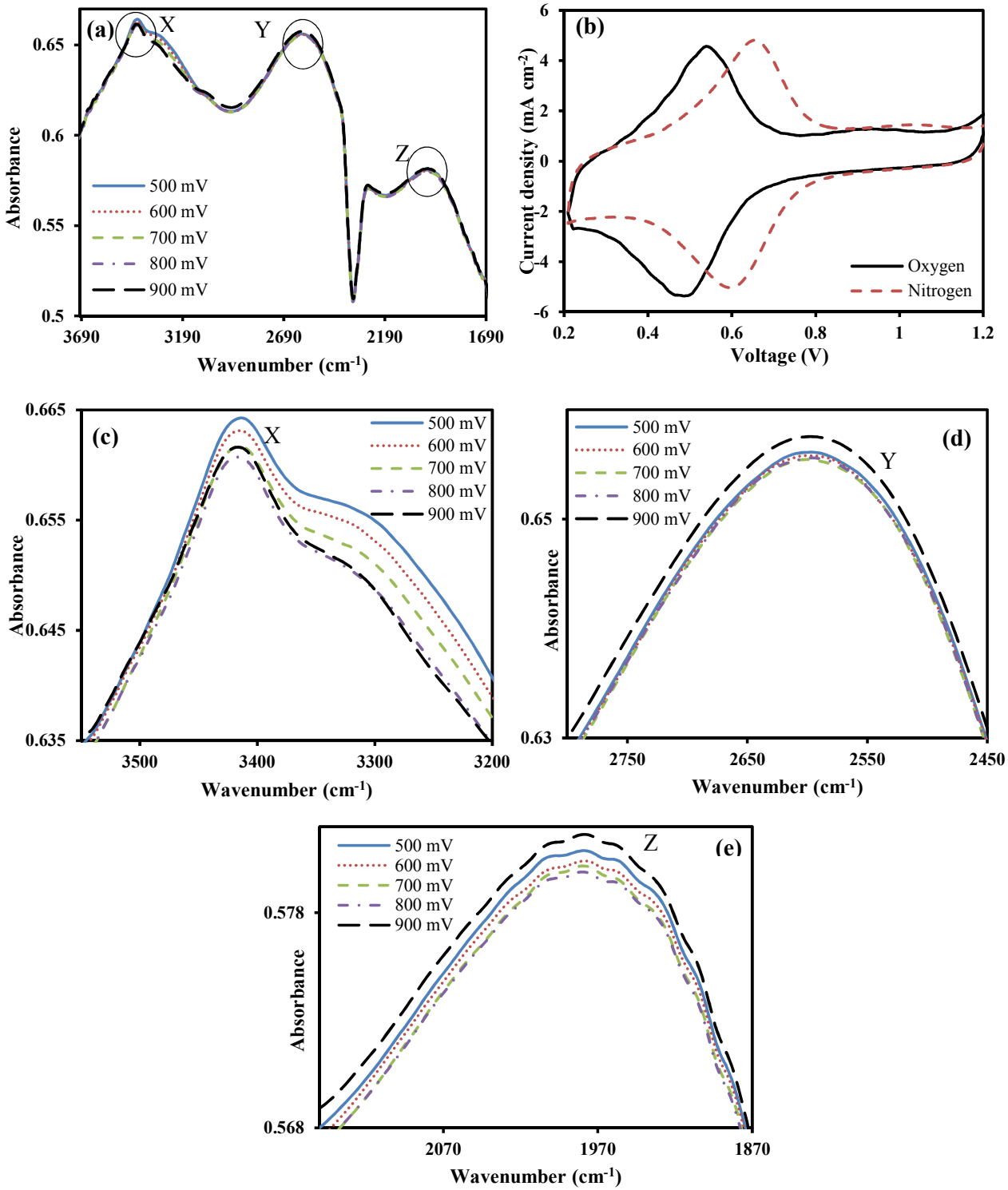

Figure 7: (a) *In-situ* FTIR spectra at potentials 0.9 V, 0.8 V, 0.7 V, 0.6 V and 0.5 V with (b) cyclic voltammetry of CN_x/PVA nanofibers in nitrogen and oxygen purged 0.5 M H_2SO_4 for ORR. Expanded portion of FTIR bands: (c) X at 3410 cm^{-1} (d) Y at 2590 cm^{-1} and (e) Z at 1980 cm^{-1}.

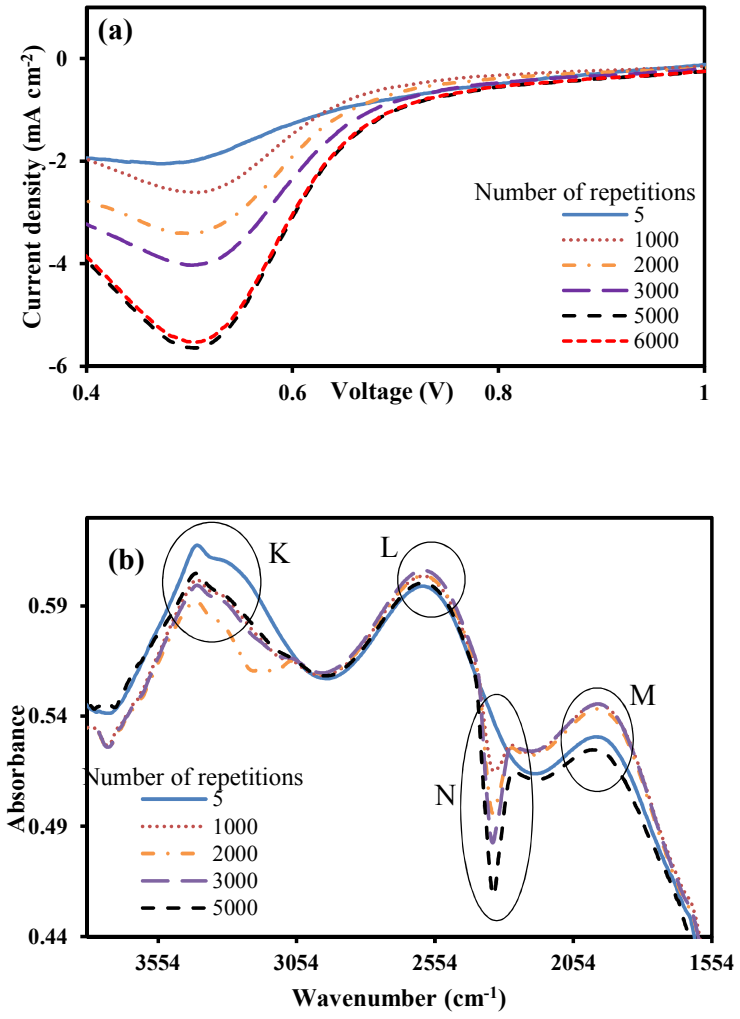

Figure 8: (a) Polarization curves of CN_x/PVA nanofibers for ORR at different LSV repetitions and (b) FTIR spectra observed at 700 mV at different LSV repetitions.

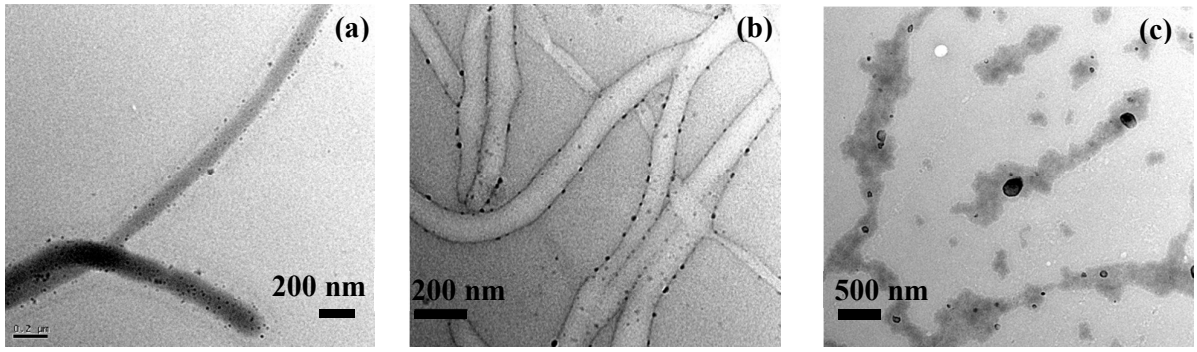

Figure 9: TEM images of CN_x/PVA nanofibers dispersed in isopropyl alcohol (c) before ORR voltammetry (d) 2000 LSV repetitions for ORR and (e) 5000 LSV repetitions for ORR

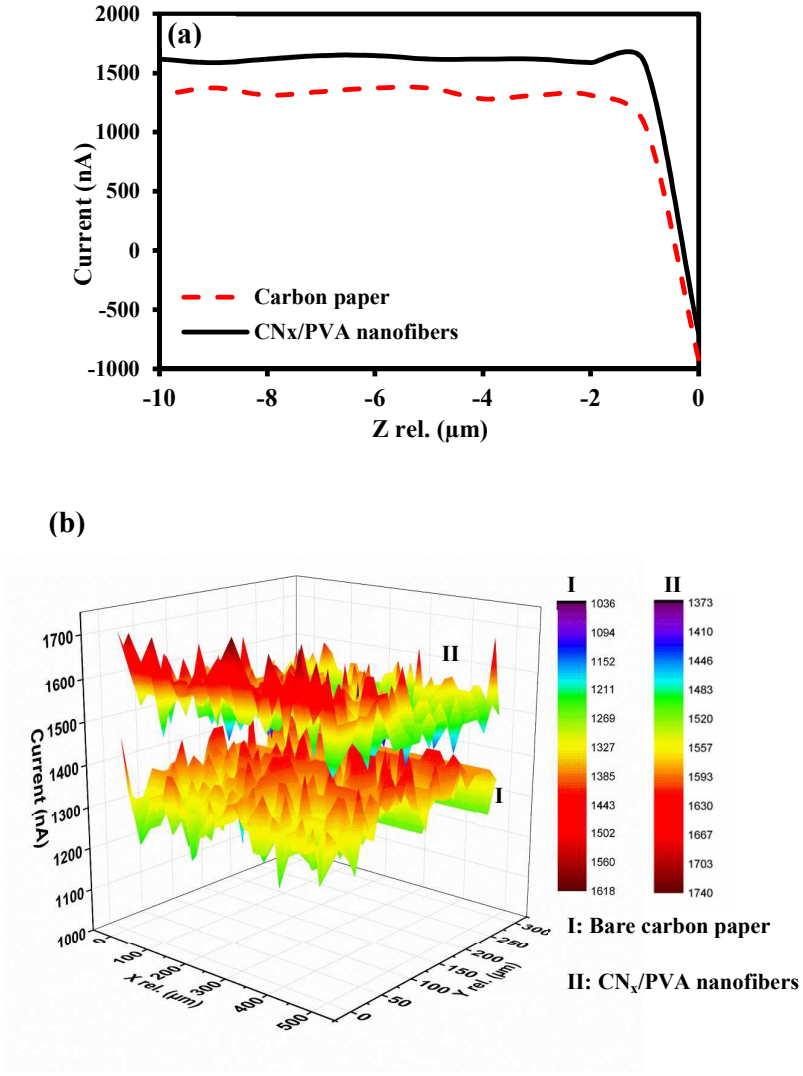

Figure 10: (a) Current-distance (approach) curve when the Pt microelectrode (25 µm) is approaching the carbon paper (CN_x/PVA nanofibers coated and uncoated) surface, (b) SECM plot showing variation of current with electrode area surface (XY) keeping the height (Z) constant